Nano Research 2018, 11(6): 3088–3095
https://doi.org/10.1007/s12274-017-1703-3
Research Article
ISSN 1998-0124
CN 11-5974/O4

A general synthetic strategy to monolayer graphene

Youqi Zhu[1,2], Tai Cao[2], Chuanbao Cao[1] (✉), Xilan Ma[1], Xingyan Xu[1], and Yadong Li[2] (✉)

[1] *Research Center of Materials Science and Beijing Key Laboratory of Construction Tailorable Advanced Functional Materials and Green Applications, Beijing Institute of Technology, Beijing 100081, China*
[2] *Department of Chemistry, Tsinghua University, Beijing 100084, China*

Received: 5 April 2017
Revised: 27 May 2017
Accepted: 8 June 2017

KEYWORDS
monolayer graphene, pyrolytic conversion, sodium carboxylate, bulk production

ABSTRACT

The emergence and establishment of new techniques for material fabrication are of fundamental importance in the development of materials science. Thus, we herein report a general synthetic strategy for the preparation of monolayer graphene. This novel synthetic method is based on the direct solid-state pyrolytic conversion of a sodium carboxylate, such as sodium gluconate or sodium citrate, into monolayer graphene in the presence of Na_2CO_3. In addition, gram-scale quantities of the graphene product can be readily prepared in several minutes. Analysis using Raman spectroscopy and atomic force microscopy clearly demonstrates that the pyrolytic graphene is composed of a monolayer with an average thickness of ~ 0.50 nm. Thus, the present pyrolytic conversion can overcome the issue of the low monolayer contents (i.e., 1 wt.%–12 wt.%) obtained using exfoliation methods in addition to the low yields of chemical vapor deposition methods. We expect that this novel technique may be suitable for application in the preparation of monolayer graphene materials for batteries, supercapacitors, catalysts, and sensors.

1 Introduction

The discovery of new materials is highly dependent on the establishment of novel synthetic techniques [1]. For example, pulsed laser vaporization gave rise to the discovery of C_{60}, whereas arc-discharge evaporation was used to produce carbon nanotubes [2, 3]. In addition, the first isolation of monolayer graphene by a facile mechanical cleavage technique not only revealed the abundance of different carbon allotropes, but also began a revolution in materials science and technology that is now coming into a two-dimensional (2D) age [4]. This atomically thin 2D nanostructure has since opened up an emerging research field of new materials, and has attracted significant attention owing to its potential properties [5–7]. However, these predicted properties can only be observed depending on the availability of specific preparation techniques [8]. To date, many synthetic techniques have been developed to prepare monolayer graphene. Although mechanical exfoliation was initially employed, this process suffers from low yields, and hence, is only suitable for small-scale research use [9, 10]. In addition, liquid exfoliation and the reduction of graphene oxide have been widely

Address correspondence to Chuanbao Cao, cbcao@bit.edu.cn; Yadong Li, ydli@mail.tsinghua.edu.cn

used for the bulk preparation of monolayer graphene [5, 11, 12]; however, these methods also suffer from particularly low yields [5], and the products tend to have a significant number of defects [13–16]. Furthermore, although chemical vapor deposition (CVD) has been developed for monolayer graphene preparation [17–20], this method requires the use of a high-temperature gas phase process and catalytic metal substrates, which renders it expensive and gives a rather low output [21]. The development of a scalable synthetic technique for the economic preparation of high quality monolayer graphene is therefore of particular interest, despite its challenges [22–24].

In this context, the pyrolytic conversion of organic molecules is an efficient route to the bulk production of various carbon materials. For example, three-dimensional (3D) highly oriented pyrolytic graphite (HOPG) was first obtained from the pyrolysis of polyacrylonitrile in the presence of montmorillonite [25]. In principle, 2D graphene can also be prepared through this pyrolytic conversion route. Indeed, Tour et al. reported the pyrolytic preparation of monolayer graphene from a poly(methyl methacrylate) thin film on a Cu substrate [26]. However, the quantities of substrate required limits large-scale production and results in high overall costs [27]. Thus, there is a serious requirement for technical innovation in the development of a pyrolytic conversion method for monolayer graphene preparation in analogy to that employed for bulk HOPG production. In this context, we herein report the development of a novel direct pyrolytic conversion approach for the gram-scale preparation of high-quality monolayer graphene from sodium carboxylate in the presence of Na_2CO_3. We expect that the proposed methodology may lead to the development of a simple and convenient route for the bulk preparation of monolayer graphene and will inevitably promote its practical application to ultimately boost advances in carbon-related physics, chemistry, and materials science.

2 Experimental

All reagents employed herein were commercially available and of analytical grade. Sodium gluconate ($C_6H_{11}NaO_7$, 99.0%) was purchased from Tianjin Fu Chen Chemical Reagents Factory (Tianjin, China). Sodium citrate ($Na_3C_6H_5O_7{\cdot}2H_2O$, 99.0%), sodium carbonate (Na_2CO_3, 99.0%), hydrochloric acid (HCl, 99.0%), and ethanol (C_2H_6O, 99.0%) were purchased from Beijing Chemical Works (Beijing, China). All reagents were used as received without further purification.

Monolayer graphene was prepared via a general direct solid-state pyrolytic conversion method from a range of different precursors. We will now take its conversion from sodium gluconate as an example. In a typical procedure, sodium gluconate (10.907 g) and Na_2CO_3 powder (105.99 g) were ground thoroughly in a 1:20 molar ratio using an agate mortar and pestle. The resulting mixture was placed in a corundum boat and transferred into a corundum tube mounted in a traditional horizontal tube furnace (55 cm length, 5 cm diameter). After flushing with a flow of Ar for 30 min, the reactor was heated to 950 °C at a heating rate of 3 °C·min^{-1} and held at this temperature for 10 min. The system was then allowed to cool naturally to room temperature under a flow of Ar. To remove any remaining traces of the Na_2CO_3 salt, treatment with dilute hydrochloric acid was carried out. Finally, the pyrolysis products were purified by washing with distilled water and absolute ethanol during vacuum filtration until the filtrate gave a neutral pH value. Subsequent drying at 80 °C for 12 h yielded the pure monolayer graphene powder (7.37 g, 51.4%).

The crystalline structure and phase purity of the as-synthesized monolayer graphene were identified by X-ray diffractometry (XRD; Bruker D8, Cu$K\alpha$ source, λ = 1.54178 Å). The morphology and microstructure of the product were observed by field emission scanning electron microscopy (FESEM, Hitachi S-4800) and transmission electron microscopy (TEM, JSM-2100F, 200 kV). High-resolution TEM and high angle annular dark field scanning transmission electron microscopy (HAADF-STEM) were performed on a FEI Tecnai G2 F20 microscope at an accelerating voltage of 200 kV. Nitrogen adsorption–desorption isotherms were performed on a Micromeritics ASAP 2020 surface area analyzer (Micromeritics Instruments, USA) at 77 K up to 1 bar pressure to evaluate the porous structure and the specific surface area of the obtained monolayer graphene. Before carrying out the adsorption measure-

ments, the solid graphene powder was degassed over 8 h at 423 K under vacuum to remove any adsorbed gases or moisture. The Brunauer–Emmett–Teller (BET) surface area was then calculated according to the multi-point BET theory, and the porosity distribution was confirmed using the adsorption data based on the Barrett–Joyner–Halenda (BJH) model. X-ray photoelectron spectroscopy (XPS) was performed on a PHI Quanteral II instrument (PHI, Japan, Al Kα = 280.00 eV). The binding energies were calibrated by referencing the C 1s peak to 284.6 eV. Atomic force microscopy (AFM) analysis was performed in tapping mode under an air atmosphere using a Multimode Nanoscope IIIa SPA (Veeco Instruments, Bruker, Germany), and the final image was flattened using Nanoscope Analysis software (version 1.40). Prior to the AFM observations, the monolayer graphene was initially dispersed in ethanol by ultrasonic processing overnight and then placed on a silicon wafer. Raman spectra were obtained using a Renishaw inVia™ confocal Raman microscope (Renishaw, England). The averaged Raman data were collected over 1 cm^2 of the sample using a 632.8 nm excitation laser with an intensity of 5 mW. The dried monolayer graphene powder was used directly for Raman measurements.

The electrochemical performance of the monolayer graphene for lithium storage applications was then evaluated using a two-electrode system composed of a lithium metal counter, a Celgard 2400 membrane separator, and a 1 M $LiPF_6$ electrolyte. The working electrode was composed of 70 wt.% monolayer graphene, 15 wt.% Super P, and 15 wt.% polyvinylidene fluoride (PVDF) binder supported by a Cu current collector. A LAND CT2001A battery testing system (Hannuo Electronics Co., Ltd. China) was used to test the charge–discharge performance between 0.01 and 3.0 V vs. Li/Li^+ at a current density of 100 $mA{\cdot}g^{-1}$.

3 Results and discussion

We initially selected commercially available sodium gluconate as a solid carbon source for the preparation of monolayer graphene. Figure 1(a) shows the monolayer graphene sample (~ 7.37 g) obtained from 43.62 g of this precursor, with the excellent yield (51.4%) indicating the potential for the bulk production of monolayer graphene. In addition, the Raman spectrum (Fig. 1(b)) exhibits three key signals at 1,325, 1,580, and 2,655 cm^{-1}, which were assigned to the D, G, and 2D bands, respectively. The sharp nature of all Raman peaks suggests enhanced quality graphene compared to that of reduced graphene oxide. Furthermore, the observed G-band associated with the stretching eigenmode of the C–C bond in graphitic materials reveals a typical sp^2-hybridized carbon network. Moreover, the 2D band exhibits a single symmetric Lorentzian peak with a full-width at half maximum of ~ 49 cm^{-1} and a 2D/G intensity ratio of 1.43:1, which confirms that the pyrolytic graphene is indeed monolayer graphene [17]. The presence of sp^3 carbon atoms or defects/disorder in the monolayer lattice structure was also indicated by the presence of the low intensity D-band, where the G/D intensity ratio of ~ 2.67:1 reveals a ~ 70 nm distance between defects in the graphene lattice [28]. The obtained Raman data therefore imply that the quality of the obtained monolayer graphene is comparable to that of CVD graphene.

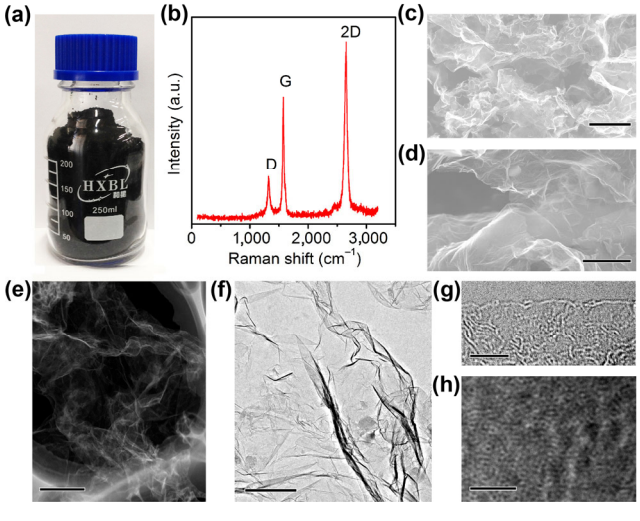

Figure 1 Structure of the monolayer graphene prepared from a sodium gluconate precursor. (a) Photographic image of the 7.37 g sample in a 250 mL bottle. (b) The Raman spectrum of the monolayer graphene. (c) and (d) Typical FESEM images (scale bars = 2 μm and 500 nm, respectively). (e) HADF-STEM image (scale bar = 500 nm). (f) Bright-field TEM image (scale bar = 200 nm) and an inset showing the selected area electron diffraction (SAED) pattern (scale bar = 2 1/nm). (g) HRTEM image recorded from the edge region of a single graphene sheet (scale bar = 5 nm). (h) HRTEM image recorded from the central area of a single graphene sheet (scale bar = 2 nm).

As indicated in Figs. 1(c)–1(f) and Fig. S1 in the Electronic Supplementary Material (ESM), the prepared monolayer graphene displays a geometrical sheet-like 2D microstructure with a micron-sized planar area. In addition, the graphene sheet is highly flexible and transparent towards the SEM beam, thereby revealing its ultrathin nature. Thus, these results indicate that following heat treatment at 950 °C for 10 min, the sodium gluconate precursor was completely pyrolyzed and converted into the 2D carbon nanostructure with a layer morphology yield of ~ 100% (Fig. 1(c) and Fig. S1(a) in the ESM). Furthermore, the atomically thin graphene can exist in a free-standing state. Although the individual graphene sheet exhibits a large number of ripples (Figs. S1(b) and S1(c) in the ESM), the intrinsic formation of the observed corrugations may be responsible for its stability. The graphene sheet also exhibits relatively sharp cuts and a well-defined outline with a rather flat surface close to the edge region due to the edge effect of the sheet structure (Fig. 1(d) and Fig. S1(d) in the ESM). As an atomically thin single layer 2D carbon structure, the free-standing monolayer graphene exhibits a significantly stronger tendency towards various regional out-of-plane deformations than a bilayer or similar structure. As further shown in the HADF-STEM image (Fig. 1(e)), the monolayer graphene is slightly wrinkled rather than being perfectly flat. It has been reported that the wrinkling of graphene sheets could result in the formation of fold lines that not only stabilize the 2D structure, but also enhance its electrical conductivity [29]. As such, this wrinkled structure could provide an excellent platform for preparing various graphene-based architectures for use in a wide range of applications. The highly transparent nature of the monolayer graphene product is further demonstrated by the STEM and TEM images given in Figs. 1(e) and 1(f). As shown in the TEM image, the homogeneous and featureless regions reveal the flat monolayer graphene sheet, whereas the less transparent areas correspond to the folding and overlapped areas, and the dark belts originate from the fold lines. The folded regions located at the edge could also be employed to determine the number of layers in the graphene structure [30, 31]. Figure 1(g) shows the high-resolution TEM (HRTEM) image detected at the edge region, which indicates that a single line is present, thereby confirming the presence of a monolayer. In addition, an HRTEM image from the central area of the monolayer graphene sheet is shown in Fig. 1(h). In this case, a rough surface texture is observed, consisting of a single layer of irregular atomic rings, which differs significantly from the surfaces of layered graphene that exhibit hexagonal lattices or lattice fringes [32]. The observed rough monolayer graphene can therefore be attributed to the appearance of lattice defects, such as carbon deficiencies and disordered segments.

The sheet-like morphology of the obtained graphene product was also confirmed by AFM imaging (Fig. 2(a)). In addition, Fig. 2(b) shows the corresponding height profiles randomly recorded along the lines marked (1), (2), and (3) in the AFM image. The average thickness was determined to be ~ 0.50 nm, which is slightly greater than the theoretical interlayer spacing (~ 0.34 nm) in graphite, but is within the reported range of 0.5–1.0 nm for monolayer graphene supported by a silicon wafer [33]. Combination of these observations with the aforementioned Raman and HRTEM results allowed us to conclude that the pyrolytic carbon sheet is indeed monolayer graphene. Furthermore, analysis by XPS confirmed that the monolayer graphene contains

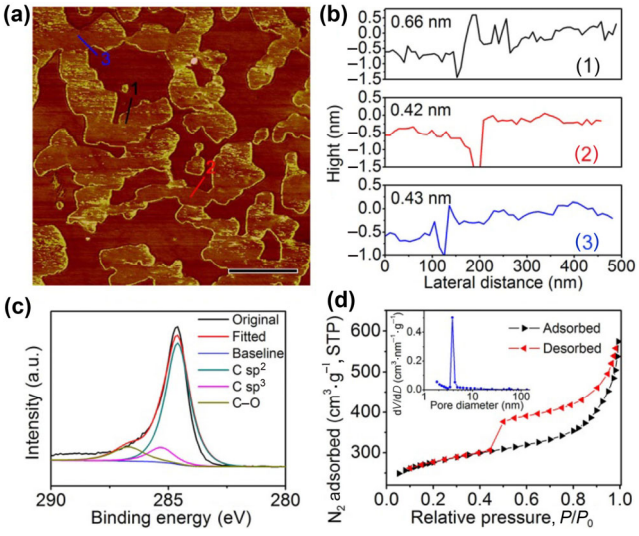

Figure 2 Thickness, composition, and surface area of the monolayer graphene prepared from a sodium gluconate precursor. (a) AFM image (scale bar = 1 μm). (b) Corresponding height profiles. (c) High-resolution XPS analysis of the C1s region and deconvolution of the C1s peak. (d) Nitrogen adsorption–desorption isotherms and an inset showing the corresponding pore-size distribution.

only C and O, with a carbon concentration of ~ 92.8%, which is indicative of the high purity of this pyrolytic graphene (Fig. S2 in the ESM). As shown in Fig. 2(c), the C1s region of the monolayer graphene could be deconvoluted into three components centered at 284.9, 285.7, and 286.8 eV, which correspond with sp^2 carbon, sp^3 carbon, and C–O moieties, respectively [29]. The content of sp^2 carbon atoms was calculated to be ~ 77.7% according to the fitted peak areas, which reveals the relatively high quality of the graphene product. We expect that the observed sp^3-bonded carbon atoms may originate from defective dangling bonds. With respect to the one-atom thick structure, the most distinguishing feature of graphene is related to its ultrahigh theoretical surface area (i.e., 2,600 $m^2 \cdot g^{-1}$). Thus, we investigated the porous structure and specific surface area of the prepared monolayer graphene. As indicated in Fig. 2(d), the obtained isotherms reveal a mesoporous structure with slit-shaped pores, which could be created by ripples or morphological restacking of the graphene sheets. In addition, the monolayer graphene in the solid powder state exhibits a high multi-point BET surface area of 915 $m^2 \cdot g^{-1}$; however, this is significantly lower than the theoretical value. We expect that this suppressed intrinsic BET surface area is due to the wrinkled structure or to agglomeration [34]. In contrast, use of the methylene blue (MB) adsorption technique gives a surface area of 1,989 $m^2 \cdot g^{-1}$ when dispersed in an ethanol suspension of the graphene powder. This apparent surface area variation is likely due to the dissipation of free sheets in the dilute solution in contrast to the solid state.

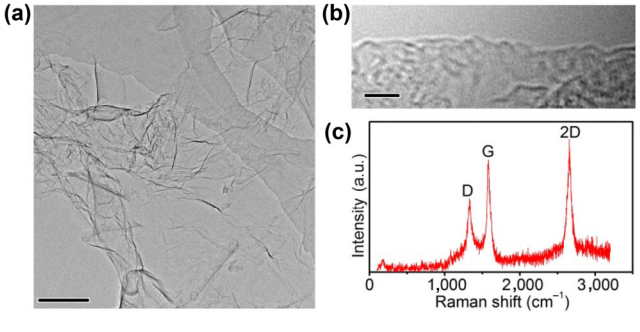

Figure 3 Characterization of the monolayer graphene obtained from a sodium citrate precursor. (a) Typical bright-field TEM image (scale bar = 200 nm). (b) HRTEM image recorded from the edge region of a single graphene sheet (scale bar = 2 nm). (c) Raman spectrum.

Given that the new synthetic strategy for monolayer graphene preparation is based on a general pyrolytic conversion, a broad range of solid carbon-contained precursors can be used as feedstocks. We therefore examined the use of sodium citrate and sodium oleate as alternative carbon sources. The 2D morphological features of the monolayer graphene prepared directly from sodium citrate were confirmed by TEM, as shown in Fig. 3(a), and HRTEM (Fig. 3(b)) also confirmed that this product is indeed monolayer graphene. In addition, the Raman spectrum shown in Fig. 3(c) clearly reveals the three key Raman scattering features of monolayer graphene, as described previously. Furthermore, according to the XPS measurements (Fig. S3 in the ESM) the carbon atom concentration is 93.0% and the sp^2 carbon content is ~ 74.9%. The obtained monolayer graphene also exhibits a high multi-point BET surface area of 785 $m^2 \cdot g^{-1}$ (Fig. S4 in the ESM), while the MB adsorption surface area was determined to be 2,121 $m^2 \cdot g^{-1}$. These results therefore confirm that the novel synthetic strategy is suitable for the general preparation of monolayer graphene from a range of substrates.

As shown in Fig. 4, the primary reaction taking place during the preparation of monolayer graphene via the general solid-state pyrolytic conversion method involves thermal cyclodehydration and in-plane carbon reconstruction. Upon heating, the sodium carboxylate monomers become covalently cross-linked in the Na_2CO_3 medium and eliminate water molecules and Na^+ through a cyclodehydration reaction. Initially, the highly polarized covalent bond between the carboxyl carbon and its nearby carbon atom is broken, resulting in the formation of disordered carbonaceous radicals, which may consist of cyclized carbon atoms. The ionic sodium species is then released in the form of Na_2CO_3 crystals (Fig. S5 in the ESM). At elevated temperatures, the cyclized carbon atoms are rearranged in the 2D direction, thereby producing a single graphene layer. Generally, the pyrolytic conversion from the sp^3 bonded carbon atoms into the sp^2 network always leads to the formation of amorphous carbon fragments. However, in the present heat-treatment system, the Na_2CO_3 phase exhibits strong interactions with the carbon π-electron species, and thus drives the cyclized carbonaceous radicals towards in-plane rearrangement. We herein

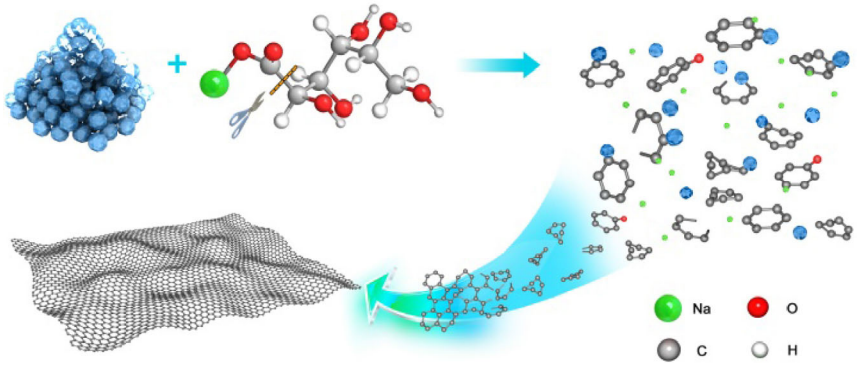

Figure 4 Schematic outline of the general solid-state pyrolytic conversion strategy for preparation of the monolayer graphene. The blue spheres represent the Na_2CO_3 salt, the large green sphere represents Na^+ in the solid sodium carboxylate precursor, and the small green spheres represent the Na_2CO_3 crystals generated *in situ*.

selected sodium carboxylate as the solid carbon-containing precursor, not only due to its low cost and excellent availability, but also due to the inherent ionic sodium species present in the original framework. The *in-situ* generated Na_2CO_3 clusters were evenly distributed within the carbon matter, thereby allowing for full contact, which is responsible for the complete conversion from carbonaceous radicals to monolayer graphene.

Novel synthetic techniques in the field of carbon material fabrication science are usually distinguished by new discoveries and innovations. For example, Tomita et al. used lamellar montmorillonites as 2D reactors for preparing HOPG for the first time, which gave rise to a number of practical applications [25]. In this case, we found that Na_2CO_3 played a crucial role in the formation of monolayer graphene, as the pyrolysis behavior of solid-state organic precursors can be regulated in the presence of the added and converted Na_2CO_3 phase. In practice, the inorganic Na_2CO_3 salt could enhance the dehydration and cross-linking reactions and increases the carbon yield [35]. In addition, the required conversion temperature in the Na_2CO_3-assisted system could be reduced to 800 °C (Figs. S6(a)–S6(f) in the ESM, which is equal to the growth temperature required for Cu catalysts [25] and lower than most reported values (≥ 1,000 °C) for the CVD and epitaxial growth methods [17–21, 36]. Such a low processing temperature is therefore highly desirable and favorable for industrial production. Moreover, removal of the final Na_2CO_3 was straightforward via a simple acid treatment method, thereby allowing a high purity product to be obtained. Thus, the use of an alkali metal carbonate is preferable to the use of using other inorganic additives in preparing the pyrolytic carbon. More importantly, our novel substrate-free processing technique could overcome the limitation of growth substrates in the CVD process, thereby rendering it possible to prepare monolayer graphene in large (i.e., ton-scale) quantities.

These results suggest that the direct conversion of solid carbon sources appears to be a promising route towards bulk graphene fabrication. In contrast, gas phase processes (e.g., CVD) tend to result in low carbon yields, whereas in the direct solid-state conversion method, the carbon loss can be reduced significantly [37, 38]. In this case, the carbon yield was calculated to be ~ 51.4% based on the total carbon atom content in the sodium gluconate precursor. In addition, the CVD process is based on the catalytic pyrolysis of small molecule precursors, and is limited to gaseous carbon sources such as methane and acetylene [39]. In contrast, our novel pyrolytic conversion technique should allow the use of a wider variety of potential raw materials. Indeed, the use of other sodium carboxylates is currently under investigation. We also expect that a range of sodium-free solid carbon sources, such as resins, polymers, and biomass, may also be suitable for use as feedstocks if thoroughly mixed with Na_2CO_3. The resulting monolayer graphene is therefore more likely to find a large variety of practical applications. For example, when employed as an anode in lithium-ion batteries, monolayer graphene exhibits a high reversible capacity of 782.1 $mAh \cdot g^{-1}$

over 200 cycles (Fig. S7 in the ESM), which is higher than that of other layered graphene structure prepared by alternative methods. These results indicate that monolayer graphene exhibits great potential for use as a commercial electrode material for electrochemical lithium storage applications.

4 Conclusions

In conclusion, we successfully developed a general synthetic strategy for the preparation of monolayer graphene based on a direct solid-state pyrolytic conversion of sodium carboxylates (i.e., sodium gluconate and sodium citrate) in the presence of Na_2CO_3. The proposed primary reaction consists of thermal cyclodehydration and in-plane carbon reconstruction, where the Na_2CO_3 phase has a beneficial effect on the pyrolytic conversion. We report the gram-scale (i.e., 7.37 g) preparation of the desired monolayer graphene for the first time, representing a 51.4% yield. This direct solid-state pyrolytic conversion strategy overcomes the drawbacks of traditional exfoliation and chemical vapor deposition methods, and thus should be considered a promising alternative synthetic strategy. We expect that the prepared monolayer graphene will be suitable for a range of practical applications, including as a commercial electrode material for electrochemical lithium storage applications. We also believe that a newfound enthusiasm for pyrolytic monolayer graphene can be expected, as the development of our novel synthetic technique should promote its use in various materials science applications. Studies on the use of other sodium carboxylates are currently underway, and the results will be presented in due course.

Acknowledgements

The authors gratefully thank the National Natural Science Foundation of China (No. 21371023) and the National Key Basic Research Program of China (No. 2015CB251100).

Electronic Supplementary Material: Supplementary material (morphology and microstructure characterization measurements and electrochemical performances measurements) is available in the online version of this article at https://doi.org/10.1007/s12274-017-1703-3.

References

[1] Wang, X.; Zhuang, J.; Peng, Q.; Li, Y. D. A general strategy for nanocrystal synthesis. *Nature* **2005**, *437*, 121–124.

[2] Kroto, H. W.; Heath, J. R.; O'Brien, S. C.; Curl, R. F.; Smalley, R. E. C_{60}: Buckminsterfullerene. *Nature* **1985**, *318*, 162–163.

[3] Iijima, S. Helical microtubules of graphitic carbon. *Nature* **1991**, *354*, 56–58.

[4] Novoselov, K. S.; Geim, A. K.; Morozov, S. V.; Jiang, D.; Zhang, Y.; Dubonos, S. V.; Grigorieva, I. V.; Firsov, A. A. Electric field effect in atomically thin carbon films. *Science* **2004**, *306*, 666–669.

[5] Hernandez, Y.; Nicolosi, V.; Lotya, M.; Blighe, F. M.; Sun, Z. Y.; De, S.; McGovern, I. T.; Holland, B.; Byrne, M.; Gun'Ko, Y. K. et al. High-yield production of graphene by liquid-phase exfoliation of graphite. *Nat. Nanotech.* **2008**, *3*, 563–568.

[6] Raccichini, R.; Varzi, A.; Passerini, S.; Scrosati, B. The role of graphene for electrochemical energy storage. *Nat. Mater.* **2015**, *14*, 271–279.

[7] Yang, L. M.; Bačić, V.; Popov, I. A.; Boldyrev, A. I.; Heine, T.; Frauenheim, T.; Ganz, E. Two-dimensional Cu_2Si monolayer with planar hexacoordinate copper and silicon bonding. *J. Am. Chem. Soc.* **2015**, *137*, 2757–2762.

[8] Kawai, S.; Eren, B.; Marot, L.; Meyer, E. Graphene synthesis via thermal polymerization of aromatic quinone molecules. *ACS Nano* **2014**, *8*, 5932–5938.

[9] Georgakilas, V.; Perman, J. A.; Tucek, J.; Zboril, R. Broad family of carbon nanoallotropes: Classification, chemistry, and applications of fullerenes, carbon dots, nanotubes, graphene, nanodiamonds, and combined superstructures. *Chem. Rev.* **2015**, *115*, 4744–4822.

[10] Park, S.; Ruoff, R. S. Chemical methods for the production of graphenes. *Nat. Nanotech.* **2009**, *4*, 217–224.

[11] Stankovich, S.; Dikin, D. A.; Dommett, G. H. B.; Kohlhaas, K. M.; Zimney, E. J.; Stach, E. A.; Piner, R. D.; Nguyen, S. T.; Ruoff, R. S. Graphene-based composite materials. *Nature* **2006**, *442*, 282–286.

[12] Xu, M. W.; Sun, H. T.; Shen, C.; Yang, S.; Que, W. X.; Zhang, Y.; Song, X. P. Lithium-assisted exfoliation of pristine graphite for few-layer graphene nanosheets. *Nano Res.* **2015**, *8*, 801–807.

[13] Paton, K. R.; Varrla, E.; Backes, C.; Smith, R. J.; Khan, U.; O'Neill, A.; Boland, C.; Lotya, M.; Istrate, O. M.; King, P. et al. Scalable production of large quantities of defect-free

few-layer graphene by shear exfoliation in liquids. *Nat. Mater*. **2014**, *13*, 624–630.

[14] Cote, L. J.; Cruz-Silva, R.; Huang, J. X. Flash reduction and patterning of graphite oxide and its polymer composite. *J. Am. Chem. Soc*. **2009**, *131*, 11027–11032.

[15] Stankovich, S.; Dikin, D. A.; Piner, R. D.; Kohlhaas, K. A.; Kleinhammes, A.; Jia, Y. Y.; Wu, Y.; Nguyen, S. T.; Ruoff, R. S. Synthesis of graphene-based nanosheets via chemical reduction of exfoliated graphite oxide. *Carbon* **2007**, *45*, 1558–1565.

[16] Eda, G.; Fanchini, G.; Chhowalla, M. Large-area ultrathin films of reduced graphene oxide as a transparent and flexible electronic material. *Nat. Nanotech*. **2008**, *3*, 270–274.

[17] Li, X. S.; Cai, W. W.; An, J.; Kim, S.; Nah, J.; Yang, D. X.; Piner, R.; Velamakanni, A.; Jung, I.; Tutuc, E. et al. Large-area synthesis of high-quality and uniform graphene films on copper foils. *Science* **2009**, *324*, 1312–1314.

[18] Berger, C.; Song, Z. M.; Li, X. B.; Wu, X. S.; Brown, N.; Naud, C.; Mayou, D.; Li, T. B.; Hass, J.; Marchenkov, A. N. et al. Electronic confinement and coherence in patterned epitaxial graphene. *Science* **2006**, *312*, 1191–1196.

[19] Huang, H.; Chen, W.; Chen, S.; Wee, A. T. S. Bottom-up growth of epitaxial graphene on 6H-SiC (0001). *ACS Nano* **2008**, *2*, 2513–2518.

[20] Zhang, L. C.; Shi, Z. W.; Liu, D. H.; Yang, Rong.; Shi, D. X.; Zhang, G. Y. Vapour-phase graphene epitaxy at low temperatures. *Nano Res*. **2012**, *5*, 258–264.

[21] Oliveira Jr, M. H.; Lopes, J. M. J.; Schumann, T.; Galves, L. A.; Ramsteiner, M.; Berlin, K.; Trampert, A.; Riechert, H. Synthesis of quasi-free-standing bilayer graphene nanoribbons on SiC surfaces. *Nat. Commun*. **2015**, *6*, 7632.

[22] Chen, L.; Hernandez, Y.; Feng, X. L.; Müllen, K. From nanographene and graphene nanoribbons to graphene sheets: Chemical synthesis. *Angew. Chem., Int. Ed*. **2012**, *51*, 7640–7654.

[23] Lee, M. J.; Choi, J. S.; Kim, J. S.; Byun, I. S.; Lee, D. H.; Ryu, S.; Lee, C.; Park, B. H. Characteristics and effects of diffused water between graphene and a SiO_2 substrate. *Nano Res*. **2012**, *5*, 710–717.

[24] Li, X. H.; Kurasch, S.; Kaiser, U.; Antonietti, M. Synthesis of monolayer-patched graphene from glucose. *Angew. Chem., Int. Ed*. **2012**, *51*, 9689–9692.

[25] Kyotani, T.; Sonobe, N.; Tomita, A. Formation of highly orientated graphite from polyacrylonitrile by using a two-dimensional space between montmorillonite lamellae. *Nature* **1988**, *331*, 331–333.

[26] Sun, Z. Z.; Yan, Z.; Yao, J.; Beitler, E.; Zhu, Y.; Tour J. M. Growth of graphene from solid carbon sources. *Nature* **2010**, *468*, 549–552.

[27] Wang, X. B.; Zhang, Y. J.; Zhi, C. Y.; Wang, X.; Tang, D. M.; Xu, Y. B.; Weng, Q. H.; Jiang, X. F.; Mitome, M.; Golberg, D. et al. Three-dimensional strutted graphene grown by substrate-free sugar blowing for high-power-density supercapacitors. *Nat. Commun*. **2013**, *4*, 2905.

[28] Ferrari, A. C.; Basko, D. M. Raman spectroscopy as a versatile tool for studying the properties of graphene. *Nat. Nanotech*. **2013**, *8*, 235–246.

[29] Zhu, W. J.; Low, T.; Perebeinos, V.; Bol, A. A.; Zhu, Y.; Yan, H. H.; Tersoff, J.; Avouris, P. Structure and electronic transport in graphene wrinkles. *Nano Lett*. **2012**, *12*, 3431–3436.

[30] Dato, A.; Radmilovic, V.; Lee, Z.; Phillips, J.; Frenklach, M. Substrate-free gas-phase synthesis of graphene sheets. *Nano Lett*. **2008**, *8*, 2012–2016.

[31] Ferrari, A. C.; Meyer, J. C.; Scardaci, V.; Casiraghi, C.; Lazzeri, M.; Mauri, F.; Piscanec, S.; Jiang, D.; Novoselov, K. S.; Roth, S. et al. Raman spectrum of graphene and graphene layers. *Phys. Rev. Lett*. **2006**, *97*, 187401.

[32] Meyer, J. C.; Geim, A. K.; Katsnelson, M. I.; Novoselov, K. S.; Booth, T. J.; Roth, S. The structure of suspended graphene sheets. *Nature* **2007**, *446*, 60–63.

[33] Tang, Y. B.; Lee, C. S.; Chen, Z. H.; Yuan, G. D.; Kang, Z. H.; Luo, L. B.; Song, H. S.; Liu, Y.; He, Z. B.; Zhang, W. J. et al. High-quality graphenes via a facile quenching method for field-effect transistors. *Nano Lett*. **2009**, *9*, 1374–1377.

[34] Li, D.; Müller, M. B.; Gilje, S.; Kaner, R. B.; Wallace, G. G. Processable aqueous dispersions of graphene nanosheets. *Nat. Nanotech*. **2008**, *3*, 101–105.

[35] Zheng, S. K.; Feng, J. W.; Maciel, G. E. *In situ* high-temperature electron paramagnetic resonance (EPR) investigation of the charring of cellulose and cellulose/Na_2CO_3 mixtures and the O_2-induced and H_2O-induced behaviors of these chars. *Energy Fuels* **2005**, *19*, 1201–1210.

[36] Lee, S.; Lee, K.; Zhong, Z. H. Wafer scale homogeneous bilayer graphene films by chemical vapor deposition. *Nano Lett*. **2010**, *10*, 4702–4707.

[37] Chen, J. W.; Cui, M. Q.; Wu, G. X.; Wang, T. Y.; Mbengue, J. M.; Li, Y. F.; Li, M. C. Fast growth of large single-crystalline graphene assisted by sequential double oxygen passivation. *Carbon* **2017**, *116*, 133–138.

[38] Li, Y. F.; Li, M. C.; Gu, T. S.; Bai, F.; Yu, Y.; Trevor, M.; Yu, Y. X. An important atomic process in the CVD growth of graphene: Sinking and up-floating of carbon atom on copper surface. *Appl. Surf. Sci*. **2013**, *284*, 207–213.

[39] Li, Y. F.; Li, M. C.; Wang, T.; Bai, F.; Yu, Y. X. DFT study on the atomic-scale nucleation path of graphene growth on the Cu(111) surface. *Phys. Chem. Chem. Phys*. **2014**, *16*, 5213–5220.